Electronic Supplementary Material (ESI) for Nanoscale Horizons.

Supplementary Information

"*Ion sliding*" on graphene: novel concept to boost supercapacitor performance

Sebastiano Bellani,[a] Beatriz Martín-García,[a] Reinier Oropesa-Nuñez,[a,b] Valentino Romano,[a,c] Leyla Najafi,[a] Cansunur Demirci,[d] Mirko Prato,[e] Antonio Esau Del Rio Castillo,[a] Luigi Marasco,[a] Elisa Mantero,[a] Giovanna D'Angelo[c] and Francesco Bonaccorso[a,b]*

[a] *Graphene Labs, Istituto Italiano di Tecnologia, via Morego 30, 16163 Genova, Italy.*

[b] *BeDimensional Srl., Via Albisola 121, 16163 Genova, Italy*

[c] *Dipartimento di Scienze Matematiche ed Informatiche, Scienze Fisiche e Scienze della Terra, Università di Messina, Viale F. Stagno D'Alcontres 31, 98166 Messina, Italy*

[d] *NanoChemistry, Istituto Italiano di Tecnologia, via Morego 30, 16163 Genova, Italy*

[e] *Materials Characterization Facility, Istituto Italiano di Tecnologia, via Morego 30, 16163 Genova, Italy*

Wet-jet milling apparatus and process

Figure S1 reports the schematic illustration of the wet-jet milling (WJM) apparatus,[1,2] showing the flow of the WJM-exfoliation process (as detailed in Experimental section of the main text). The close-up view of the processor is also illustrated. The detailed description of the WJM apparatus and process is reported in the main text (Experimental section).

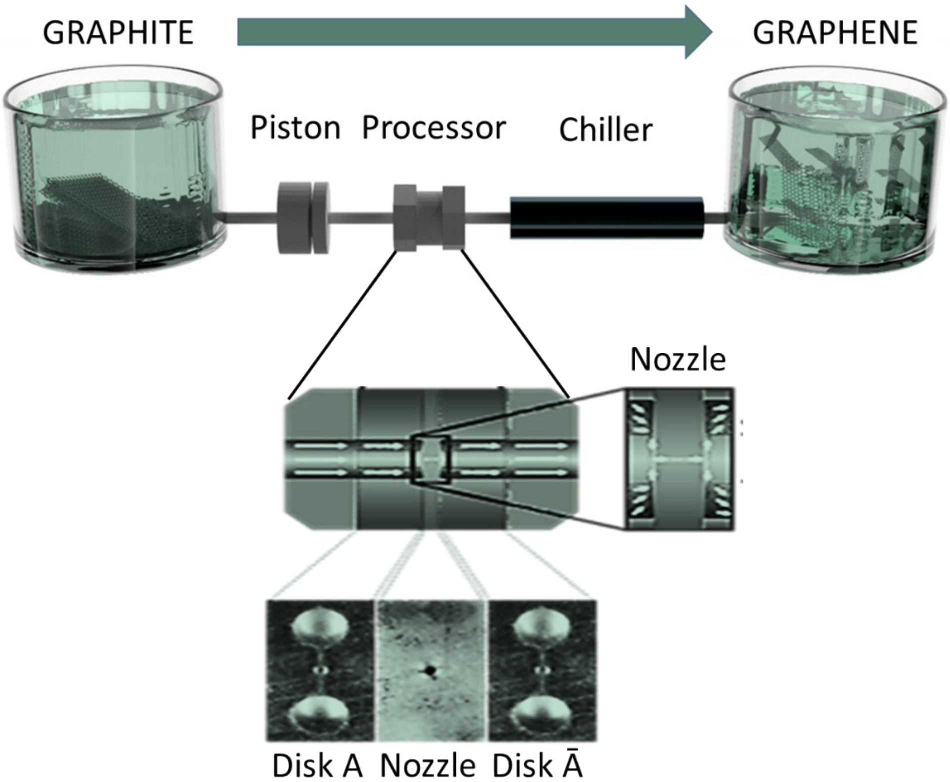

Figure S1. Schematic illustration of the wet-jet milling (WJM) apparatus and process, comprising three main building blocks: the piston, the processor and the chiller. The close-up view of the processor is also shown. The zoomed parts of the processor show the channels configuration and the disks arrangement. The fluid path is indicated by the white arrows. On the right side, a top view of the holes and channels on each disk. The disks A and Ā have two holes of 1 mm in diameter, separated by a distance of 2.3 mm from centre to centre and joined by a half-cylinder channel of 0.3 mm in diameter. The thickness of the disks A and Ā is 4 mm. The disk B consists of a 0.10 mm nozzle and it is the core of the system. The thickness of the disk B is 0.95 mm.

Raman statistical analysis of the WJM-produced single- and few-layer graphene flakes

The Raman spectrum of graphene produced by liquid phase exfoliation shows, as fingerprints, G (~1585 cm^{-1}[3,4]), D (~1380 cm^{-1}[1],[2]), D' (~1620 cm^{-1}[5]) and 2D (~2700 cm^{-1}[4]) peaks.[4,6,7,8,9,10] The G peak, positioned at ∼1585 cm^{-1}, corresponds to the E_{2g} phonon at the Brillouin zone centre.[4,6] The D peak is due to the breathing modes of sp^2 rings and requires a defect for its activation by double resonance.[3,11,12] Double resonance happens as an intra-valley process, *i.e.,* connecting two points belonging to the same cone around K or K',[4,6,7] giving origin to the D' peak.[4,6, 7] The 2D peak is the second order of the D peak, [4,6,7] and it appears also in the absence of D peak, since no defects are required for the activation of two phonons with the same momentum, one backscattered from the other.[13,14] Moreover, the 2D peak is a excitation wavelength-dependent single peak (centred at ∼2680 cm^{-1} at excitation wavelength of 514 nm) for single-layer graphene (SLG),[6,4,7] whereas is a superposition of multiple components, the main being the $2D_1$ and $2D_2$ components, for few-layers graphene (FLG).[4,6,7] In graphite, the intensity of the $2D_2$ band is twice the $2D_1$ band,[4,6,15] while for graphene the 2D band is a single and sharp Lorentzian band,[6] which is roughly four times more intense than the G peak.[6] Taking into account the intensity ratio between $2D_1$ and $2D_2$ –$I(2D_1)/(I(D_2)$–, it is possible to estimate the flake thickness.[16]

Figure S2 reports the Raman spectroscopy analysis of the measurements performed on the wet-jet mill (WJM)-produced SLG/FLG flakes. Figure S1a shows that I(D)/I(G) ranges from 0.1 to 1.2. Pos(G) and FWHM(G) range from 1578 to 1583 cm^{-1} (Figure S1b) and from 14 to 25 cm^{-1} (Figure S1c), respectively.

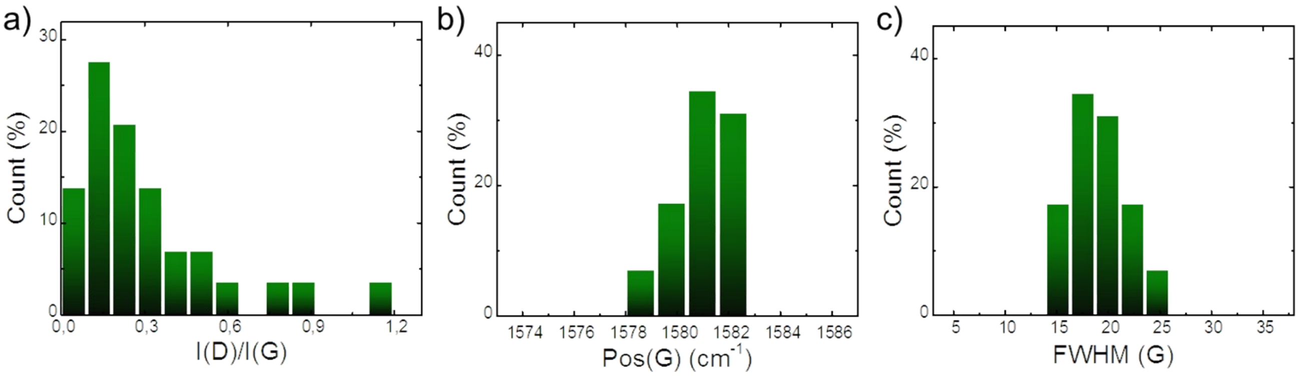

Figure S2. Raman statistical analysis or WJM-produced SLG/FLG flakes. a) I(D)/I(G); b) Pos(G); c) FWHM(G).

X-ray photoelectron spectroscopy of WJM-produced SLG/FLG flakes

X-ray photoelectron spectroscopy (XPS) measurements were carried out on the as-produced flakes to ascertain their chemical composition. **Figure S3** reports the C 1s spectrum of WJM-SLG/FLG flakes, which can be decomposed into different components. The main one peaks at 284.4 eV and is referred to as C=C (sp^2) of graphene flakes,[17,18,19] with the corresponding feature due to π-π* interactions at 290.8 eV.[17,18,19] The component centred at 284.8 eV refers to the C-C (sp^3)[19,20] and is due to flake edges and organic solvent residuals, as well as to environmental contaminations (adventitious carbon).[21] The other two weak contributions peaking at binding energies of 286.3 eV and 287.7 eV, can be ascribed to C-N (or C-O) and C=O groups, respectively.[22,23] Their origin is ascribed to residual NMP molecules,[22,23] whose presence is confirmed by the N 1s spectrum (inset to Figure S3) at 400.0 eV corresponding to amide groups (-N-(C=O)). These results proved that WJM technique is effective for producing SLG/FLG dispersion in NMP, in agreement with our previous studies.[1]

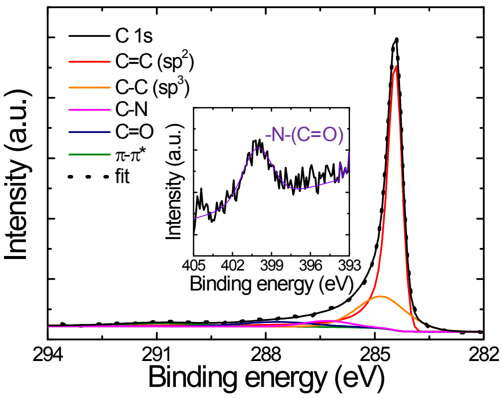

Figure S3. X-ray photoelectron spectroscopy analysis of WJM-produced SLG/FLG flakes. C 1s and N 1s (inset panel) spectra of the SLG/FLG flakes. In the main panel**,** the C 1s spectrum deconvolution is also shown, evidencing the bands ascribed to C=C, C-C, C-N, C=O and π-π*.

Morphology analysis of the supercapacitor electrodes

Figure S4 reports the morphology analyses of the supercapacitor (SC) electrodes. More in detail: panels a-e show representative cross-sectional SEM images of the SC electrodes; panels f-j report the Kr physisorption isotherm curves, Brunauer, Emmett and Teller (BET) plots (inset panels) and specific surface area calculated by BET analysis (SSA_{BET}) of the electrodes; panels k-o display the pore size distributions and D-values (D10, D20 AND D90, corresponding to the intercepts for 10%, 20% and 90% of the cumulative mass) of the electrodes. The detailed discussion of the data is reported in the main text (Supercapacitors fabrication and characterization section).

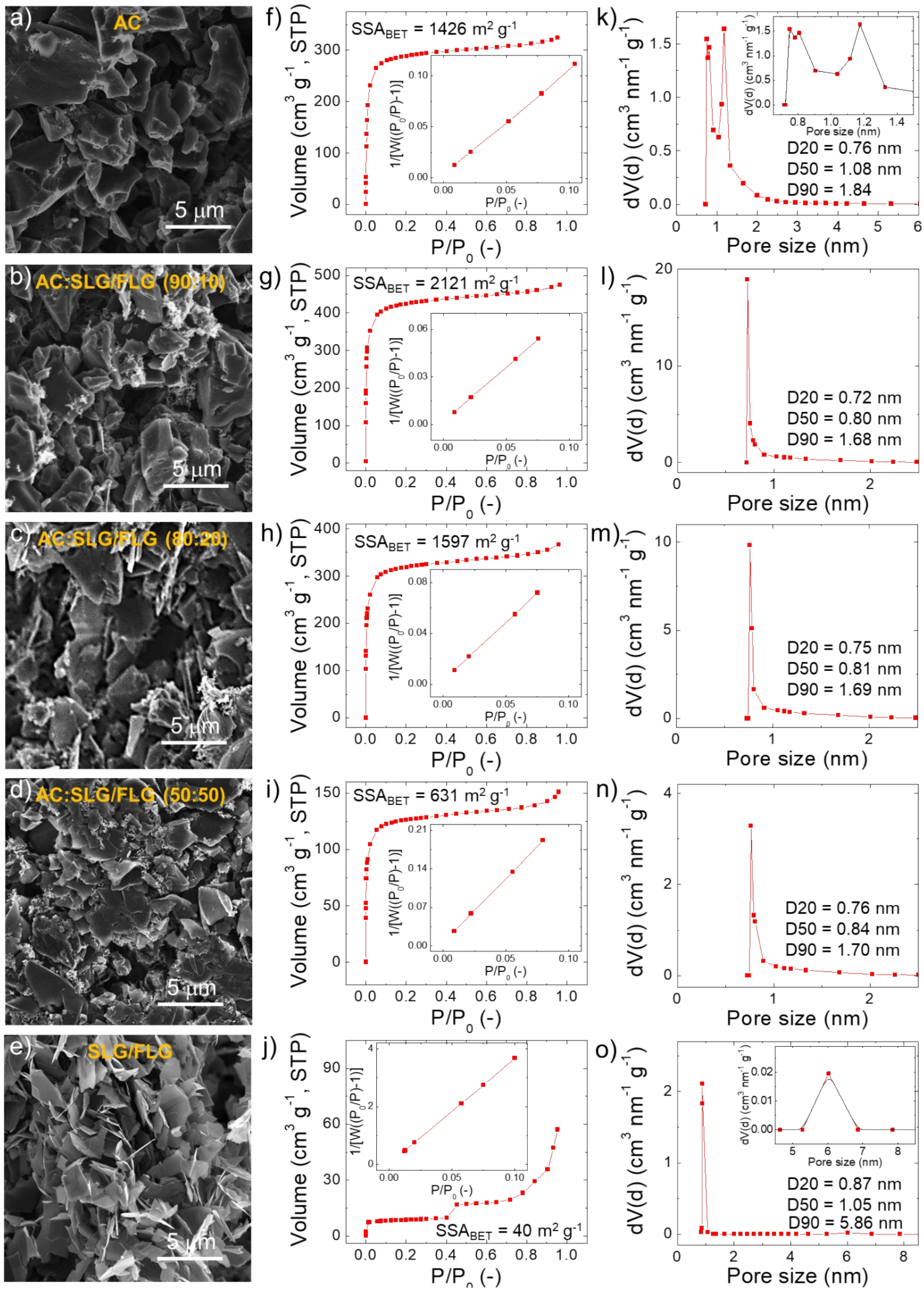

Figure S4. Morphology analysis of SC electrodes. Cross-sectional SEM images of a) AC, b) AC:SLF/FLG (90:10), c) AC:SLG/FLG (80:20), d) AC:SLG/FLG (50:50) and e) SLG/FLG electrodes. f-j) Kr physisorption isotherm curves, BET plots (inset panels) and calculated SSA$_{BET}$ of the electrodes. k-o) Pore size distributions and D-values (D20, D50 and D90, corresponding to the intercepts for 20%, 50% and 90% of the cumulative mass) of the electrodes. The inset panels k and o show the enlargements of the pore size distribution of the graphene electrode in the pore size ranges of 0.65–1.5 nm and 4.5–8.5 nm, respectively. The measurements shown on each line correspond to the same electrodes imaged by SEM.

Supplementary cyclic voltammetry analysis

Figure S5a,b show the cyclic voltammetry (CV) curves at various voltage scan rates (ranging from 0.01 to 50 V s^{-1}) measured for SLG/FLG-based SC, which still exhibits a capacitive behaviour at a voltage scan rate as high as 50 V s^{-1}. Figure S5c shows the CV curves at 50 V s^{-1} for AC- and AC:SLG/FLG-based SCs, which display resistive performance (Figure S5c).

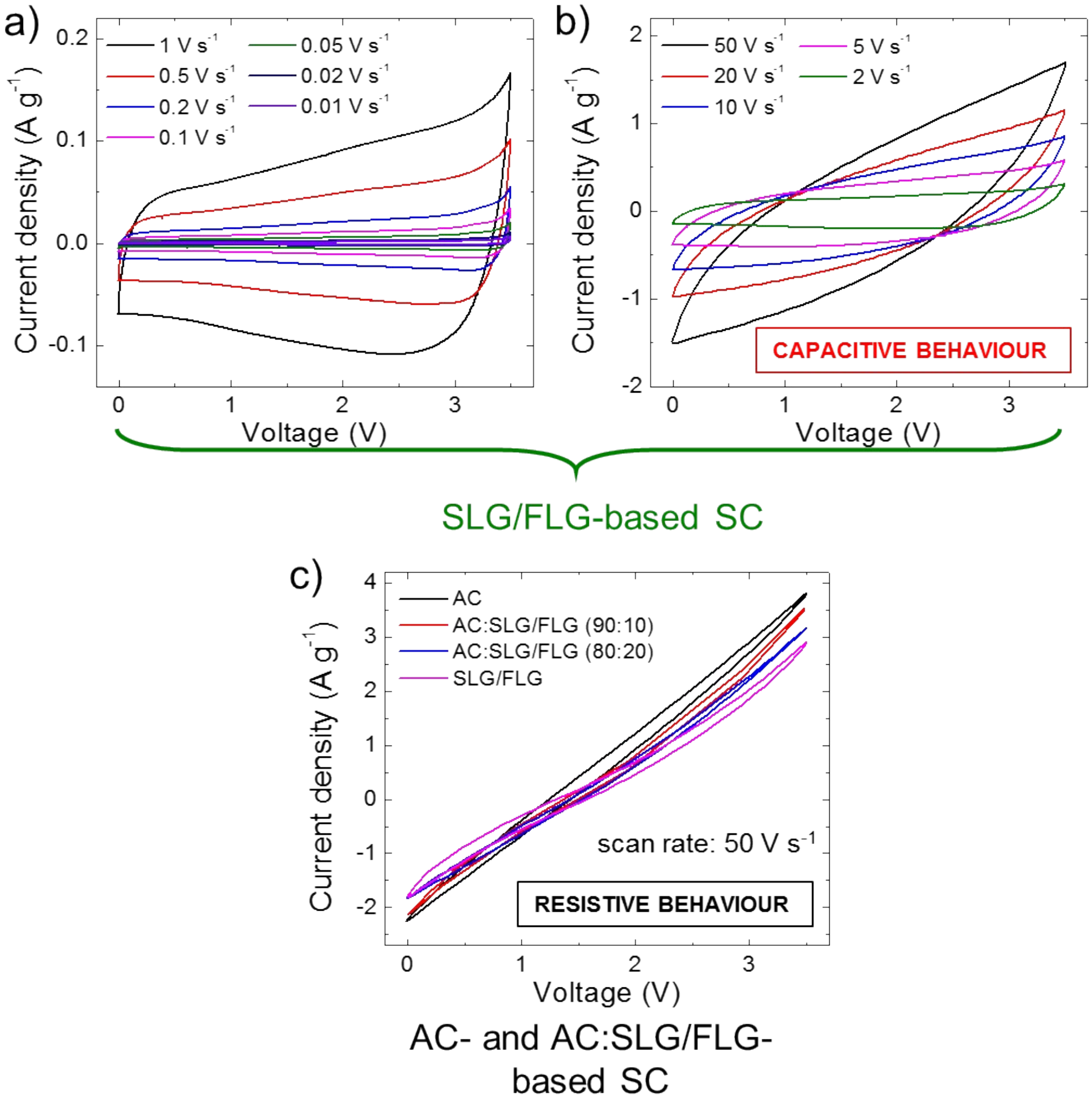

Figure S5. a,b) CV curves of SLG/FLG-based SCs at various voltage scan rates (ranging between 0.01 and 1 V s^{-1} in panel a, 2 and 50 V s^{-1} in panel b. c) CV curves of AC:SLF/FLG-based SCs at a scan rate of 50 V s^{-1}.

References

1 A. E. Del Rio Castillo, V. Pellegrini, A. Ansaldo, F. Ricciardella, H. Sun, L. Marasco, J. Buha, Z. Dang, L. Gagliani, E. Lago, N. Curreli, S. Gentiluomo, F. Palazon, P. Toth, E. Mantero, M. Crugliano, A. Gamucci, A. Tomadin, M. Polini and F. Bonaccorso, *Materials Horizons*, 2018, **5**, 890-904.

2 . Bellani, F. Wang, G. Longoni, L. Najafi, R. Oropesa-Nuñez, A. E. Del Rio Castillo, M. Prato, X. Zhuang, V. Pellegrini, X. Feng and F. Bonaccorso, *Nano Letters*, 2018, **18**, 7155-7164.

3 L. Yang, J. Deslippe, C.-H. Park, M. L. Cohen and S. G. Louie, *Physical Review Letters*, 2009, **103**, 186802.

4 A. C. Ferrari and D. M. Basko, *Nature Nanotechnology*, 2013, **8**, 235.

5 C. Y. Su, Y. Xu, W. Zhang, J. Zhao, X. Tang, C. H. Tsai and L. J. Li, *Chemistry of Materials*, 2009, **21**, 5674-5680.

6 A. C. Ferrari, J. C. Meyer, V. Scardaci, C. Casiraghi, M. Lazzeri, F. Mauri, S. Piscanec, D. Jiang, K. S. Novoselov, S. Roth and A. K. Geim, *Physical Review Letters*, 2006, **97**, 187401.

7 L. Najafi, S. Bellani, B. Martín-García, R. Oropesa-Nuñez, A. E. Del Rio Castillo, M. Prato, I. Moreels and F. Bonaccorso, *Chemistry of Materials*, 2017, **29**, 5782–5786.

8 C. Thomsen and S. Reich, *Physical Review Letters*, 2000, **85**, 5214.

9 M. S. Dresselhaus, A. Jorio, M. Hofmann, G. Dresselhaus and R. Saito, *Nano Letters*, 2010, **10**, 751–758.

10 J.-B. Wu, M.-L. Lin, X. Cong, H.-N. Liu and P.-H. Tan, *Chemical Society Reviews*, 2018, **47**, 1822–1873.

11 A. C. Ferrari and J. Robertson, *Physical Review B*, 2000, **61**, 14095–14107.

12 A. C. Ferrari and J. Robertson, *Physical Review B*, 2001, **64**, 75414.

13 C.-Y. Su, Y. Xu, W. Zhang, J. Zhao, X. Tang, C.-H. Tsai and L.-J. Li, *Chemistry of Materials*, 2009, **21**, 5674–5680.

14 S. Bellani, L. Najafi, B. Martín-García, A. Ansaldo, A. E. Del Rio Castillo, M. Prato, I. Moreels and F. Bonaccorso, *The Journal of Physical Chemistry C*, 2017, **121**, 21887–21903.

15 M. S. Dresselhaus, G. Dresselhaus and M. Hofmann, *Philosophical Transactions of the Royal Society A: Mathematical, Physical and Engineering Sciences*, 2008, **366**, 231-236.

16 D. Nuvoli, L. Valentini, V. Alzari, S. Scognamillo, S. B. Bon, M. Piccinini, J. Illescas and A. Mariani, *J. Mater. Chem.*, 2011, **21**, 3428–3431.

17 A. Siokou, F. Ravani, S. Karakalos, O. Frank, M. Kalbac and C. Galiotis, *Applied Surface Science*, 2011, **257**, 9785–9790.

18 S. Stankovich, D. A. Dikin, R. D. Piner, K. A. Kohlhaas, A. Kleinhammes, Y. Jia, Y. Wu, S. T. Nguyen and R. S. Ruoff, *Carbon*, 2007, **45**, 1558–1565.

19 J. Díaz, G. Paolicelli, S. Ferrer and F. Comin, *Physical Review B*, 1996, **54**, 8064–8069.

20 J. C. Lascovich, R. Giorgi and S. Scaglione, *Applied Surface Science*, 1991, **47**, 17–21.

21 G. Salitra, A. Soffer, L. Eliad, Y. Cohen and D. Aurbach, *Journal of The Electrochemical Society* , 2000, **147**, 2486–2493.

22 R. Buzio, A. Gerbi, S. Uttiya, C. Bernini, A. E. Del Rio Castillo, F. Palazon, A. S. Siri, V.

Pellegrini, L. Pellegrino and F. Bonaccorso, *Nanoscale*, 2017, **9**, 7612–7624.

23 H. Sun, A. E. Del Rio Castillo, S. Monaco, A. Capasso, A. Ansaldo, M. Prato, D. A. Dinh, V. Pellegrini, B. Scrosati, L. Manna and F. Bonaccorso, *J. Mater. Chem. A*, 2016, **4**, 6886–6895.